



Investigation of Boron Implantation Technique Application for Oxide Semiconductor IGZO Device Processing

Toshimasa UI*, Keisuke YASUTA, Daisuke MATSUO, Toshihiko SAKAI, Yasunori ANDOH, and Junichi TATEMICHII

Electronic devices using oxide semiconductor In-Ga-Zn-O (IGZO) are attracting attention as next-generation flat panel displays. In order to apply ion implantation technique to IGZO films, Nissin Ion Equipment Co., Ltd. and Nissin Electric Co., Ltd. performed conventional B⁺ implantation in IGZO films and investigated their optical or electrical properties. The results show that the resistance control of IGZO films by B⁺ implantation is useful for the IGZO electronic devices, especially for reducing the resistance in the source and drain region of the IGZO thin-film transistors.

Keywords: flat panel display (FPD), oxide semiconductor, IGZO, boron, ion implantation

1. Introduction

Among the electronics technologies required for the next-generation flat panel display (FPD) field, technologies that can achieve low cost, transparency, flexibility, and large area are particularly sought after. In order to realize these properties, it is necessary to make the processes simpler and lower in temperature, and develop transparent materials and flexible substrates. Indium gallium zinc oxide (IGZO), which is currently expected to be used in next-generation FPDs, is a semiconductor consisting of oxides: indium (In), gallium (Ga), zinc (Zn), and oxygen (O). It has characteristics that enable highly integrated circuits in addition to flexible, transparent, and low-power-consumption displays, and is the subject of extensive research and development for application in next-generation FPDs.

Recently, thin-film transistors (TFTs) using IGZO fabricated in vacuum processes have achieved high-speed operation, low power consumption, and high breakdown voltage.^{(1),(2)} Furthermore, in order to improve the performance of IGZO TFTs, lowering resistance in the source and drain regions by plasma irradiation,⁽³⁾ excimer laser irradiation,⁽⁴⁾ and ion implantation^{(5),(6)} have been studied, and their effectiveness has been reported. Among these technologies, the ion implantation method has advantages in terms of finer geometries, larger packing densities, and productivity; however, the mechanism of lowering resistance has not been fully elucidated. The reason for this is that there are many ion species that can be implanted, and the behavior for resistance reduction does not simply depend on atomic or molecular mass or ion valence, making the elucidation difficult. Our large ion implanters for FPD manufacturing, which are capable of implanting many ion species, are no exception and have potential process applications for a variety of requirements. To further expand the range of application, we are investigating technologies to control the sheet resistance of IGZO

thin films through ion implantation.

In this paper, we focus on boron ions (B⁺), which are conventionally used in ion implantation technology for existing silicon processes, and report on the results of our research and analysis of ion implantation in IGZO thin films deposited on glass substrates.

2. Investigation of Ion Implantation Elemental Technologies

2-1 Evaluation of sheet resistance of ion implanted IGZO thin films

We prepared an IGZO thin film with a thickness of approximately 50 nm and a sheet resistance R_s of approximately 10^{12} Ω /sq. deposited on a transparent glass substrate (thickness: 0.5 mm) using a plasma sputtering system.⁽⁷⁾ We implanted various ion species in the IGZO thin films using an ion implanter⁽⁸⁾ at an average implantation depth of approximately 15 nm and an implantation dose of 1×10^{15} ions/cm², and then evaluated R_s by Hall measurement at room temperature. Figure 1 shows the R_s measurement results of IGZO thin films without implantation and after implantation of each ion species.

The results show that compared to the IGZO thin film without implantation, R_s of the IGZO thin films with implantation decreased regardless of the implanted ion species, and that implantation of B⁺, C⁺, Ne⁺ and Ar⁺ is particularly effective in reducing R_s .⁽⁹⁾⁻⁽¹²⁾ It is known that the rare gas ions Ne⁺ and Ar⁺ become neither donors nor acceptors themselves, and that the oxygen vacancy V_o produced in an IGZO thin film by implantation reduces the resistance.^{(11),(12)} Regarding implantation of B⁺ and C⁺, however, their atomic masses and valence numbers are intermediate between those of other ion species, indicating that their mechanism of reducing resistance is not simple.

This paper is based on a paper presented at IDW '21 (Proceedings of The International Display Workshops vol. 28, 2021, FLX5/FMC6-3, pp. 956-959, hereinafter, the "Presented Paper"). All quotations from the Presented Paper are copyrighted by The Institute of Image Information and Television Engineers and The Society for Information Display, and are marked ©ITE, SID 2021.

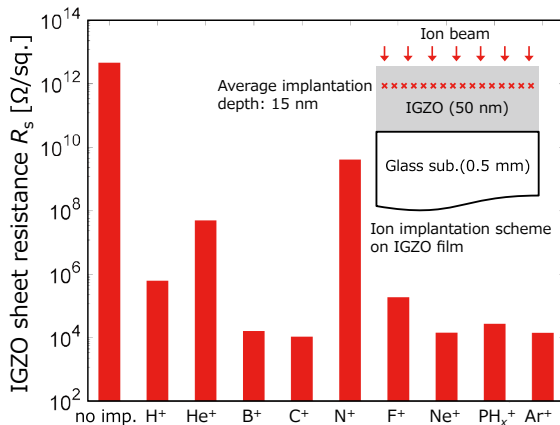


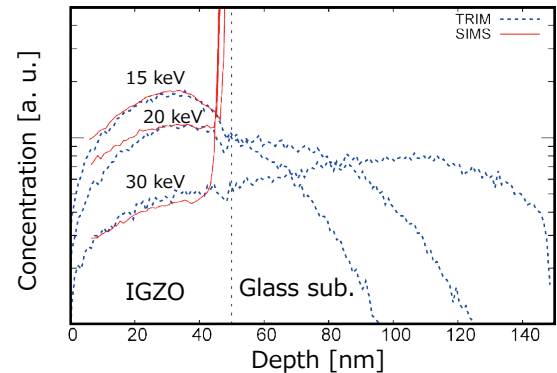
Fig. 1. Sheet resistance R_s of 50-nm-thick IGZO films with no implantation and after implantation of various ions.

2-2 Evaluation of electron transport properties of IGZO thin films with B⁺ implantation

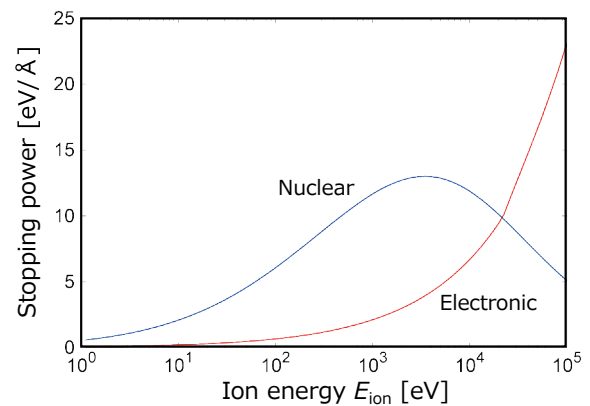
Since we found that B⁺ implantation is effective in lowering the resistance of IGZO thin films, to establish a technique for controlling the B depth profile and IGZO R_s , we implanted B⁺ in the IGZO (50 nm)/glass substrate structure with a range of ion energy E_{ion} of 15 to 30 keV. Then, we performed simulator (TRIM: Transport of Ions in Matter⁽¹³⁾) calculations and secondary ion mass spectrometry (SIMS) to obtain the depth profiles of the implanted B concentration. Figure 2 (a) indicates the obtained depth profiles of B concentration in the IGZO (50 nm)/glass substrate structure. The TRIM and SIMS profiles are consistent in the IGZO film. The B concentration profiles estimated through TRIM and SIMS are not consistent in the deeper region near the IGZO/glass substrate interface. This is due to the background of B contained in the glass substrate. Figure 2 (b) shows the stopping power for B in the IGZO estimated by SIMS and TRIM based on the B concentration profiles in the IGZO thin film (nuclear and electronic stopping powers, which represent the quantities of E_{ion} lost by the interaction of B⁺ with the atomic nucleus or electron as it travels through the IGZO thin film).

On the other hand, to optimize E_{ion} in the reduction of IGZO R_s by B⁺ implantation, we implanted B⁺ with a range of E_{ion} of 5 to 80 keV with a constant dose amount of 1×10^{15} ions/cm², and measured R_s after the implantation. Furthermore, considering the effect of heat treatment in the following processes, we prepared samples annealed in N₂ ambient or air of 250 °C for 1 hour after the B⁺ implantation, and measured R_s . The E_{ion} dependence of IGZO R_s obtained by Hall measurement is shown in Fig. 3. In the range of 10 to 20 keV, R_s decreases with increasing E_{ion} . This is due to the increase in the area of lowered resistance from the IGZO thin film surface as E_{ion} increases. In the range of 20 to 80 keV, on the other hand, R_s increases with increasing E_{ion} . This seems to be because an increase in B penetrating the IGZO thin film decreases the amount of B remaining in the IGZO thin film, as shown in Fig. 2 (a). Furthermore, we observed a greater increase/decrease behavior in the resistance after heat treatment. This suggests that B in the IGZO thin film has caused some type

of chemical reaction by heat treatment. Furthermore, the R_s differed depending on the atmosphere during heat treatment. This suggests that in the case of heat treatment in air, H₂O and O₂ act as oxidants, and Vo in the IGZO thin film, which was increased by implantation, may be reduced by



(a) Depth profiles of B concentration in the IGZO (50 nm)/glass substrate structure



(b) Stopping power for B in the IGZO

Fig. 2. Depth profiles of B concentration in the IGZO (50 nm)/glass structure of each E_{ion} and stopping power for B in the IGZO estimated by a combination of SIMS and TRIM. (Fig. 1 of the Presented Paper (©ITE, SID2021))

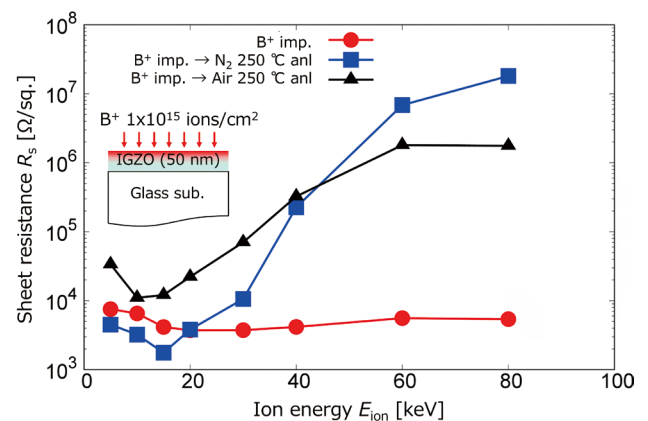


Fig. 3. Dependence of sheet resistance R_s on ion energy E_{ion} immediately after the implantation, annealing in N₂ atmosphere after the implantation, and annealing in air after B⁺ implantation into IGZO (50 nm)/glass structure with a constant implantation dose amount of 1×10^{15} ions/cm² (Fig. 2 of the Presented Paper (©ITE, SID 2021))

heat treatment. According to these results, in the insulator/IGZO structure, ion implantation can reduce the resistance of the IGZO thin film through the insulator without exposure to the air or molecules that serve as oxidants, while plasma treatment requires removal of the insulator before reducing the resistance of the IGZO thin film. This is a result that demonstrates the great advantage of ion implantation technology for IGZO device process applications.

In order to investigate the behavior of implanted B⁺ in more detail, we analyzed the depth dependence of the electron transport properties of IGZO thin films in the perpendicular direction. The analysis flow is shown in Fig. 4. We prepared an IGZO thin film with a thickness of 180 nm deposited on a glass substrate, and implanted B⁺ with E_{ion} of 50 keV with the dose amount of 1 × 10¹⁵ ions/cm². Then, we performed IGZO patterning and ohmic electrode formation. After that, we repeated the IGZO film thickness *d* evaluation by spectroscopic ellipsometry, Hall measurement, and wet etching to evaluate the electron transport properties. Figure 5 shows the obtained dependence of R_s, Hall mobility μ_{meas} and sheet carrier concentration n_{meas} on IGZO etching depth *x*. Here, *x* is estimated from the relation *x* = *t* - *d*, where *t* is the thickness at the time of IGZO deposition (180 nm). We found that R_s increases slowly when *x* < 150 nm and increases rapidly when *x* > 150 nm. Furthermore, we learned that μ_{meas} and n_{meas} decrease slowly when *x* < 150 nm and decrease rapidly when *x* > 150 nm. These results suggest that high-density electrons are generated in the *x* = 0 to 150 nm range of the IGZO thin film.

Since the above results provide only averaged electron transport properties of the remaining IGZO film after etching, in order to further quantitatively evaluate the depth information, we considered a parallel conductance model and analyzed the local electron concentration n_j and local Hall mobility μ_j profiles as functions of IGZO thin film depth. The parallel conductance model diagram is shown in Fig. 6. In this model, the conductivity of electrons flowing through the IGZO thin film in the Hall measurement is described by a composite of parallel connections in each layer.

When a weak-magnetic-field approximation (the product of mobility μ and magnetic-flux density *B*: μ*B* << 1) is applicable in the Hall measurement, simultaneous equations hold as follows:

$$\sigma_{\text{meas}} \simeq \sum_j \sigma_j, (\sigma_{\text{meas}} = n_{\text{meas}} \cdot \mu_{\text{meas}}, \sigma_j = n_j \cdot \mu_j) \dots (1)$$

$$\sigma_{\text{meas}} \cdot \mu_{\text{meas}}^2 \simeq \sum_j \sigma_j \cdot \mu_j^2 \dots \dots \dots (2)$$

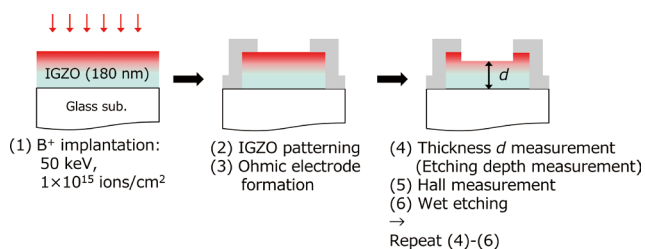


Fig. 4. Process flow of depth profile analyses of electron transport properties

where n_{meas} is the measured carrier density and μ_{meas} is the measured Hall mobility. Since in this Hall measurement, from *B* ~ 0.35 Tesla and μ ~ 10 cm²/Vs in the IGZO film, μ*B* ~ 0.00035, the weak-magnetic-field approximation μ*B* << 1 holds. Using the Hall measurement results shown in Fig. 5 and the simultaneous Eqs. (1) and (2), the n_j profile

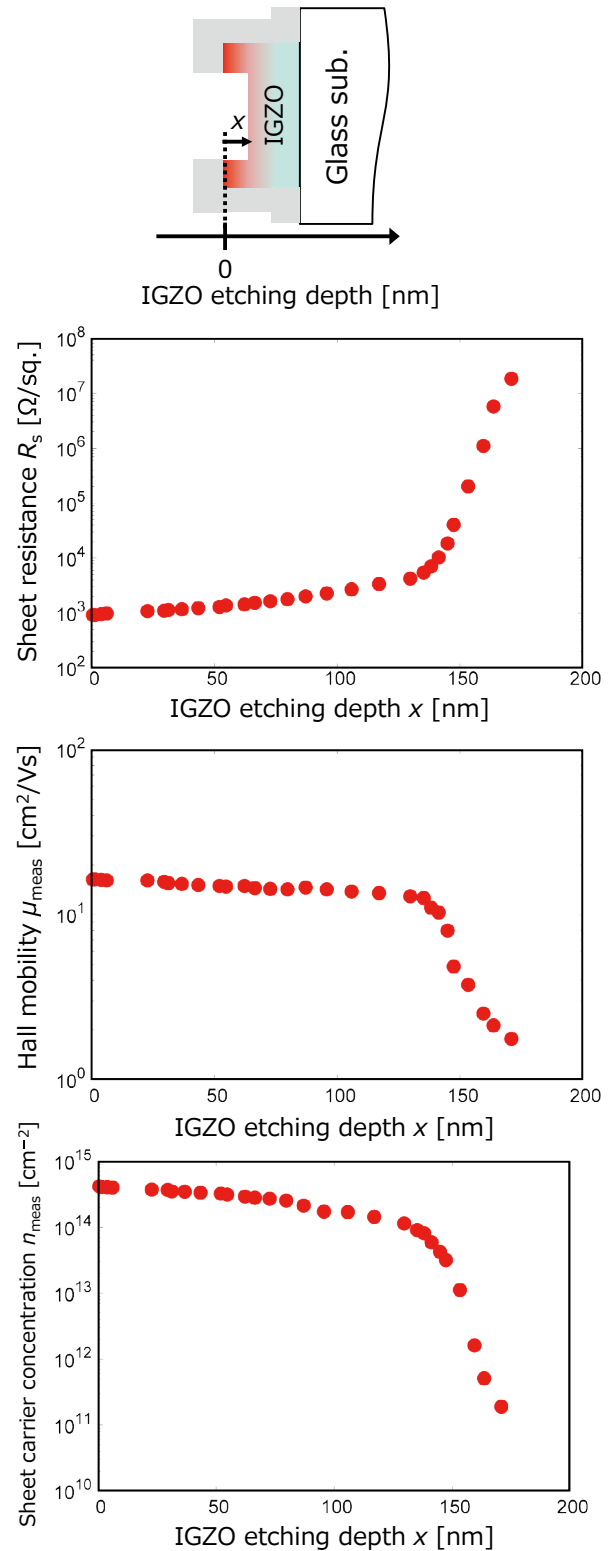


Fig. 5. Depth dependence of electron transport properties of B⁺-implanted IGZO thin films (Fig. 4 of the Presented Paper (©ITE, SID 2021))

as functions of a IGZO thin film depth is shown in Fig. 7 (a). In addition, the B concentration profile calculated by TRIM using the two stopping powers and the SIMS profile in the IGZO film shown in Fig. 2 (b) are also shown. The Vo concentration profile calculated by TRIM is also shown assuming that the binding energy of each atom constituting

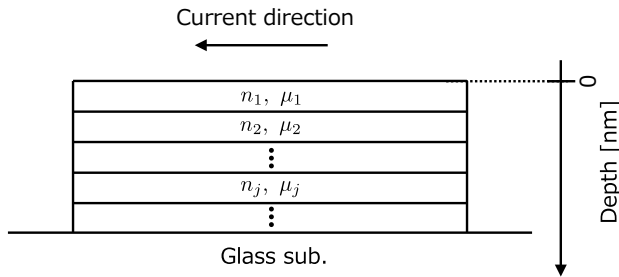


Fig. 6. Parallel conductance model diagram of local electron concentration n_j and local Hall mobility μ_j as functions of depth direction of IGZO thin film. (Fig. 5 of the Presented Paper (©ITE, SID 2021))

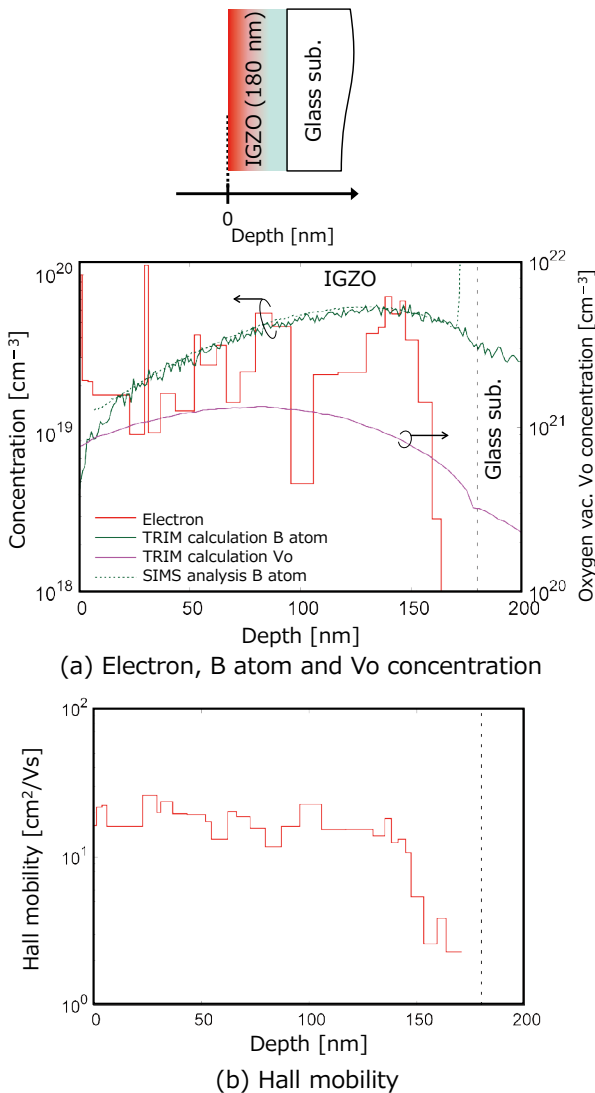


Fig. 7. Electron, Vo and B concentration profiles and Hall mobility profile as functions of depth of IGZO thin films (Fig. 6 of the Presented Paper (©ITE, SID 2021))

the IGZO thin film is a general value of ~ 3 eV. First, the TRIM calculation results for the B concentration profile in the IGZO film are in good agreement with the SIMS results. Furthermore, although a comparison of the n_j , Vo, and B concentration profiles shows that at depths < 100 nm from the IGZO surface (0 nm depth) the Vo profile producing electrons is consistent with the n_j profile, it is significantly different from the Vo profile with a peak near ~ 150 nm depth. However, the B concentration profile has a peak near ~ 150 nm, which is consistent with the Vo profile. Figure 7 (b) shows the μ_j profile calculated using the simultaneous Eqs. (1) and (2). From the depths of 0 to 150 nm, μ_j is 10 to 20 cm^2/Vs . These results suggest that B itself may contribute to reduction in resistance in IGZO films.

2-3 X-Ray photoelectron spectroscopy evaluation of B-implanted IGZO

To analyze the behavior of B in IGZO thin films from a different perspective, we evaluated the R_s reduction and the molecular bonding state of B⁺-implanted IGZO thin films. Specifically, we analyzed IGZO thin films by X-ray photoelectron spectroscopy (XPS) immediately after B⁺ implantation under the lowest R_s conditions of $E_{\text{ion}} = 15$ keV and the implantation dose = 1×10^{15} ions/ cm^2 , as shown in Fig. 3, and N₂ annealing following the implantation. For comparison, we also evaluated IGZO thin films without implantation and after N₂ annealing without implantation. The X-ray used was Al K α (1286.6 eV). Figure 8 (a) shows the obtained wide spectra. All obtained elemental spectra were identifiable, and there were no

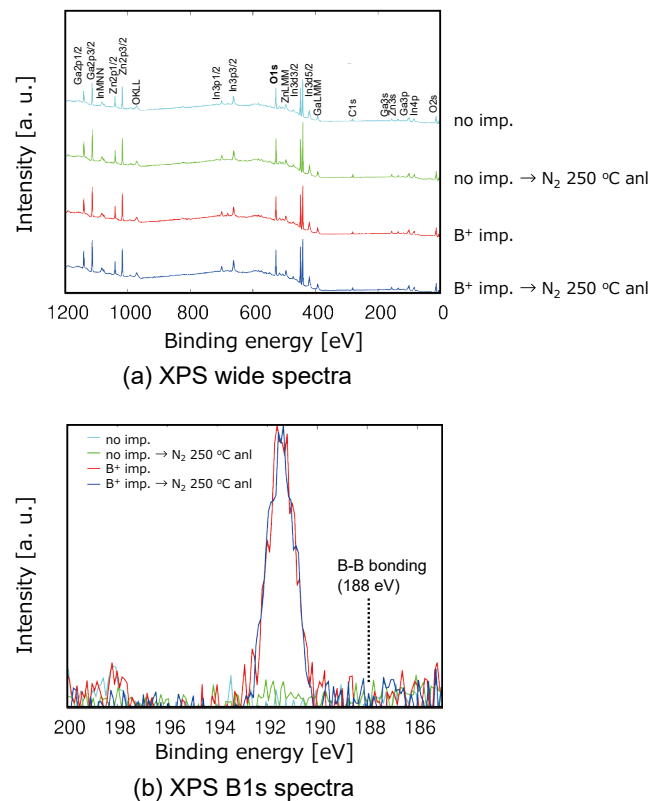


Fig. 8. X-ray photoelectron spectroscopy wide spectra and B1s spectra for IGZO thin films. (Fig. 3 of the Presented Paper (©ITE, SID2021))

elemental spectra constituting the IGZO film other than those related to implanted B and to carbon (C) deposited on the surface in air. The shift correction of the binding energy due to sample charging during the XPS measurement was performed at C1s (284.6 eV) as shown in Fig. 8 (a).

Figure 8 (b) indicates the obtained B1s spectra. For the IGZO films without implantation, no peak related to B was observed with or without annealing. On the other hand, for the B-implanted IGZO films, the peak around 192 eV was observed for both with and without annealing, where

- (1) The binding energy of B bound to B (B-B bond) is 188 eV,⁽¹⁴⁾ and the obtained binding energy is larger than that,
- (2) Electronegativity, which indicates the degree of electron attraction, is Zn (1.65) < In (1.78) < Ga (1.81) < B (2.04) < O (3.44).

Given the two facts above, the implanted B is affected by bonding with elements with a greater electronegativity than B. In other words, B is considered to be dominantly bonded to O (B-O bonding). Therefore, the combination of the electron transport properties evaluation and the XPS results suggests that B implantation not only reduces the V_o due to sputtering during implantation, but B itself also reduces the resistance of IGZO thin films. The reason why there is no significant difference in B1s with and without annealing is due to various possibilities, such as the difference between the two being buried in the measurement noise, or that the energy given off by the X-rays during measurement eliminates the difference between with and without annealing. A model diagram of R_s reduction due to B implanted into the IGZO thin film is shown in Fig. 9. While the implanted B^+ generates V_o by sputtering, the B that remains in the IGZO thin film is bound with O to break the metal atom (In, Ga, Zn)-O bonding and generate unbonded hands. It is considered that electrons with dangling bond are not localized in situ and act as carriers, reducing the IGZO R_s .

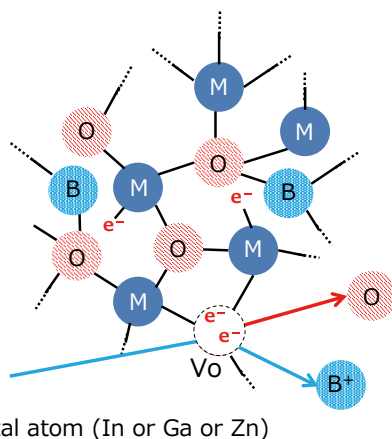


Fig. 9. Model diagram of IGZO resistance reduction by B^+ implantation.

3. Conclusion

As shown above, we reported the results of our investigation of IGZO R_s control technology by B^+ implantation for the purpose of application of ion implanters to IGZO devices—especially IGZO TFTs—in FPD technology. We used Hall measurements to analyze and evaluate optimal B^+ implantation conditions. Furthermore, we used XPS measurements to reveal that R_s can be reduced not only by V_o but also by the contribution of B itself after the implantation.

The above findings indicate that the ion implantation method is useful in the IGZO thin film device process and has the potential for further performance improvement, and we will continue its investigation.

References

- (1) K. Nomura, H. Ohta, A. Takagi, T. Kamiya, M. Hirano, and H. Hosono, *Nature* 432, 488 (2004)
- (2) T. Kamiya, K. Nomura and H. Hosono, *J. Disp. Technol.* 5, 273 (2009)
- (3) H. Jeong, B. Lee, Y. Lee, J. Lee, M. Yang, I. Kang, M. Mativenga, and J. Jang, *Appl. Phys. Lett.* 104, 022115 (2014)
- (4) M. Nakata, H. Tsuji, Y. Fujisaki, H. Sato, Y. Nakajima, T. Takei, T. Yamamoto, and T. Kurita, *Appl. Phys. Lett.* 103, 142111 (2013)
- (5) R. Chowdhury, M. Kabir, R. Manleyc, and K. Hirschman, *ECS Transactions* 92, 135 (2019)
- (6) L. Qian, W. Tang, and P. Laia, *ECS Solid State Lett.* 3, 87 (2014)
- (7) D. Matsuo, R. Miyanaga, T. Ikeda, S. Kishida, Y. Setoguchi, Y. Andoh, M. N. Fujii, and Y. Uraoka, *Proc. the 25th IDW*, 560 (2018)
- (8) S. Dohi, H. Kai, T. Nagao, T. Matsumoto, M. Onoda, K. Nakao, Y. Inouchi, J. Tatemichi, and M. Nukayama, *The Nissin Electric Review* 62, 17 (2017)
- (9) T. Ui, R. Fujimoto, K. Yasuta, D. Matsuo, T. Sakai, Y. Setoguchi, E. Takahashi, Y. Andoh and J. Tatemichi, *Proc. the 27th IDW*, 315 (2020)
- (10) K. Yasuta, T. Ui, T. Nagao, D. Matsuo, T. Sakai, Y. Setoguchi, E. Takahashi, Y. Andoh and J. Tatemichi, *Proc. the 28th IDW*, 956 (2021)
- (11) T. Ui, R. Fujimoto, T. Sakai, D. Matsuo, Y. Setoguchi, Y. Andoh, and J. Tatemichi, *Proc. the 27th AM-FPD*, 115 (2020)
- (12) K. Yasuta, T. Ui, T. Ikeda, D. Matsuo, T. Sakai, S. Dohi, Y. Setoguchi, E. Takahashi, Y. Andoh, and J. Tatemichi, *Proc. the 28th AM-FPD*, 77 (2021)
- (13) J. Ziegler and J. Biersack, *Stopping Power and Range of Ion in Matter* (2008)
- (14) A. Thompson and D. Vaughan, *X-RAY DATA BOOKLET* (2009)

Contributors The lead author is indicated by an asterisk (*).

T. UI*

- Ph.D
Nissin Ion Equipment Co., Ltd.
AM-FPD '20 Best Paper Award

**K. YASUTA**

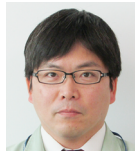
- Nissin Ion Equipment Co., Ltd.
AM-FPD '21 Poster Paper Award

**D. MATSUO**

- Ph.D
Chief Research Engineer, Nissin Electric Co., Ltd.
AM-FPD '17 ECS Japan Section Young Researcher
Award, IDW '17 Outstanding Poster Paper Award

**T. SAKAI**

- Senior Staff, Nissin Electric Co., Ltd.
IDW'18 Outstanding Poster Paper Award

**Y. ANDOH**

- Ph.D
Fellow
Nissin Electric Co., Ltd.

**J. TATEMICHI**

- Executive Engineer, Nissin Ion Equipment Co., Ltd.

